

Highlights and Perspectives of the JLab Spin Physics Program

Jian-ping Chen¹·e-mail: jpchen@jlab.org

Thomas Jefferson National Accelerator Facility, Newport News, VA 23606, USA

Abstract. Nucleon spin structure has been an active, exciting and intriguing subject of interest for the last three decades. Recent precision spin-structure data from Jefferson Lab have significantly advanced our knowledge of nucleon structure in the valence quark (high- x) region and improved our understanding of higher-twist effects, spin sum rules and quark-hadron duality. First, results of spin sum rules and polarizabilities in the low to intermediate Q^2 region are presented. Comparison with theoretical calculations, in particular with Chiral Perturbation Theory (ChPT) calculations, are discussed. Surprising disagreements of ChPT calculations with experimental results on the generalized spin polarizability, δ_{LT} , were found. Then, precision measurements of the spin asymmetry, A_1 , in the high- x region are presented. They provide crucial input for global fits to world data to extract polarized parton distribution functions. The up and down quark spin distributions in the nucleon were extracted. The results for $\Delta d/d$ disagree with the leading-order pQCD prediction assuming hadron helicity conservation. Results of precision measurements of the g_2 structure function to study higher-twist effects are presented. The data indicate a significant higher-twist (twist-3 or higher) effect. The second moment of the spin structure functions and the twist-3 matrix element d_2 results were extracted. The high Q^2 result was compared with a Lattice QCD calculation. Results on the resonance spin-structure functions in the intermediate Q^2 range are presented, which, in combination with DIS data, enable a detailed study of quark-hadron duality in spin-structure functions. Finally, an experiment to study neutron transversity and transverse spin asymmetries is discussed. A future plan with the 12 GeV energy upgrade at JLab is briefly outlined.

1 Introduction

In the last three decades the study of the spin structure of the nucleon has led to a very productive experimental and theoretical activity with exciting results and new challenges[1]. This investigation has included a variety of aspects, such as testing QCD in its perturbative regime *via* spin sum rules (like the Bjorken sum rule[2]) and understanding how the spin of the nucleon is built from the intrinsic degrees of freedom of the theory, quarks and gluons.

Recently, the high polarized luminosity available at Jefferson Lab has allowed the study of nucleon spin structure with an unprecedented precision, enabling us to access the valence quark (high- x) region[3] and also to expand the study to the second spin-structure function, g_2 [4]. Furthermore, the moments of the spin-structure functions [5] were measured [6] and the spin sum rules [6,8], polarizabilities [6] and quark-hadron duality [9,10] were studied. A new program to study the transverse spin and transverse momentum dependence in the nucleon is under way.

1.1 Inclusive polarized electron-nucleon scattering

For inclusive polarized electron scattering off a polarized nucleon target, the cross section depends on four structure functions, $F_1(Q^2, x)$, $F_2(Q^2, x)$, $g_1(Q^2, x)$ and $g_2(Q^2, x)$, where F_1 and F_2 are the unpolarized structure functions and g_1 and g_2 the polarized structure functions. In the quark-parton model, F_1 or F_2 gives the quark momentum distribution and g_1 gives the quark spin distribution. Another physics quantity of interest is the virtual photon-nucleon asymmetry A_1

$$A_1 = \frac{g_1 - (Q^2/\nu^2)g_2}{F_1} \approx \frac{g_1}{F_1}. \quad (1)$$

1.2 Moments and sum rules of the spin-structure functions

Sum rules involving the spin structure of the nucleon offer an important opportunity to study QCD. In recent years the Bjorken sum rule at large Q^2 and the Gerasimov, Drell and Hearn (GDH) sum rule [17] at $Q^2 = 0$ have attracted large experimental and theoretical [18] efforts that have provided us with rich information. A generalized GDH sum rule [19] connects the GDH sum rule with the Bjorken sum rule and provides a clean way to test theories with experimental data over the entire Q^2 range. Spin sum rules relate the moments of the spin-structure functions to the nucleon's static properties (as in Bjorken or GDH sum rules) or real or virtual Compton amplitudes, which can be calculated theoretically (as in the generalized GDH sum rule or the forward spin polarizabilities). Refs. [5,52] provide comprehensive reviews on this subject.

1.3 Spin structure in the valence quark (high- x) region

The high- x region is of special interest, because this is where the valence quark contributions are expected to dominate. With sea quark and explicit gluon contributions expected not to be important, it is a clean region to test our understanding of nucleon structure. Relativistic constituent quark models[12] should be applicable in this region and perturbative QCD[13] can be used to make predictions in the large x limit.

To first approximation, the constituent quarks in the nucleon are described by SU(6) wavefunctions. SU(6) symmetry leads to the following predictions[14]:

$$A_1^p = 5/9; \quad A_1^n = 0; \quad \Delta u/u = 2/3; \quad \Delta d/d = -1/3. \quad (2)$$

Relativistic Constituent Quark Models (RCQM) with broken SU(6) symmetry, e.g., the hyperfine interaction model[12], lead to a dominance of a 'diquark' configuration with the diquark spin $S = 0$ at high x . This implies that as $x \rightarrow 1$:

$$A_1^p \rightarrow 1; \quad A_1^n \rightarrow 1; \quad \Delta u/u \rightarrow 1; \quad \text{and} \quad \Delta d/d \rightarrow -1/3. \quad (3)$$

In the RCQM, relativistic effects lead to a non-zero quark orbital angular momentum and reduce the valence quark contributions to the nucleon spin from 1 to 0.6 – 0.75.

Another approach is leading-order pQCD [13], which assumes the quark orbital angular momentum to be negligible and leads to hadron helicity conservation. It yields:

$$A_1^p \rightarrow 1; \quad A_1^n \rightarrow 1; \quad \Delta u/u \rightarrow 1; \quad \text{and} \quad \Delta d/d \rightarrow 1. \quad (4)$$

Not only are the limiting values as $x \rightarrow 1$ important, but also the behavior in the high- x region. The behavior of A_1 as x approaches 1 is sensitive to the dynamics in the valence quark region.

1.4 The g_2 structure function and the d_2 moment

The spin structure function g_2 , unlike g_1 and F_1 , can not be interpreted in the simple quark-parton model. To understand g_2 properly, it is best to start with the operator product expansion (OPE) method. In the OPE, neglecting quark masses, g_2 can be cleanly separated into a twist-2 and a higher twist term:

$$g_2(x, Q^2) = g_2^{WW}(x, Q^2) + g_2^{H.T.}(x, Q^2) . \quad (5)$$

The leading-twist term can be determined from g_1 as[15]

$$g_2^{WW}(x, Q^2) = -g_1(x, Q^2) + \int_x^1 \frac{g_1(y, Q^2)}{y} dy , \quad (6)$$

and the higher-twist term arises from quark-gluon correlations. Therefore, g_2 provides a clean way to study higher-twist effects. In addition, at high Q^2 , the x^2 -weighted moment, d_2 , is a twist-3 matrix element and is related to the color polarizabilities [16]:

$$d_2 = \int_0^1 x^2 [g_2(x) - g_2^{WW}(x)] dx. \quad (7)$$

Predictions for d_2 exist from various models [33,34,35] and lattice QCD[36].

1.5 Quark-hadron duality in spin structure functions

Quark-hadron duality was first observed for the spin-independent structure function F_2 . In 1970, Bloom and Gilman [20] noted that the nucleon resonance data averaged to the DIS scaling curve. Recent precision data [21] confirm quark-hadron duality in the unpolarized proton structure functions. Efforts are ongoing to investigate quark-hadron duality in polarized structure functions [22]. It was predicted that in the high- x region at high enough Q^2 , the resonances will have a similar behavior as DIS. Results from HERMES [23] and CLAS [51] show the proton spin structure function g_1^p approaching duality. The study of quark-hadron duality will aid in the study of the higher-twist effects and understanding the high- x behavior in DIS.

1.6 Transversity

The transversity distributions, $\delta q(x, Q^2)$, are fundamental leading-twist (twist-2) quark distributions, similar to the unpolarized and polarized parton distributions, $q(x, Q^2)$ and $\Delta q(x, Q^2)$. In quark-parton models, they describe the net transverse polarization of quarks in a transversely polarized nucleon. There are several special features for the transversity distributions, making them uniquely interesting:

- The difference between the transversity and the longitudinal distributions is purely due to relativistic effects. In the absence of relativistic effects (as in the non-relativistic quark model, where boosts and rotations commute), the transversity distributions are identical to the longitudinally polarized distributions.
- The quark transversity distributions do not mix with gluonic effects [59] and therefore follow a much simpler evolution and have a valence-like behavior.
- The positivity of helicity amplitudes leads to the Soffer’s inequality for the transversity[60]: $|h_1^q| \leq \frac{1}{2}(f_1^q + g_1^q)$.
- The lowest moment of h_1^q measures a simple local operator analogous to the axial charge, known as the “tensor charge”, which can be calculated from lattice QCD.

Due to the chiral-odd nature of the transversity distribution, it can not be measured in inclusive DIS experiments. In order to measure $\delta q(x, Q^2)$, an additional chiral-odd object is required, such as double-spin asymmetries in Drell-Yan processes, single target-spin azimuthal asymmetries in Semi-Inclusive DIS (SIDIS) reactions, double-spin asymmetries in Λ production from e-p and p-p reactions and single-spin asymmetries in double pion production from e-p scattering. The first results, from measurements performed by the HERMES [65] and COMPASS [61] collaborations with SIDIS offered the first glimpse of possible effects caused by the transversity distributions.

2 Recent results from Jefferson Lab

The Thomas Jefferson National Accelerator Facility (Jefferson Lab, or JLab, formerly known as CEBAF - Continuous Electron Beam Accelerator Facility) is located in Newport News, Virginia, USA. The accelerator produces a continuous-wave electron beam of energy up to 6 GeV. An energy upgrade to 12 GeV is planned in the next few years. The electron beam with a current of up to 180 μA is polarized up to 85% by illuminating a strained GaAs cathode with polarized laser light. The electron beam is deflected to three experimental halls (Halls A, B and C) where the electron beam can be scattered off various nuclear targets. The scattered electrons and knocked out particles are detected in the halls with various spectrometer detector packages. The experiments reported here are from inclusive electron scattering where only the scattered electrons are detected. The neutron results presented here are from Hall A [24] where there are two High Resolution Spectrometers (HRS) with momentum up to 4 GeV/c. A polarized ^3He target, with in-beam polarization of about 50%, provides an effective polarized neutron target. The polarized luminosity reached is $10^{36} \text{ s}^{-1}\text{cm}^{-2}$. The detector package consists of vertical drift chambers (for momentum analysis and vertex reconstruction), scintillation counters (data acquisition trigger) and Čerenkov counters and lead-glass calorimeters (for particle identification (PID)). The π^- were sorted from e^- with an efficiency better than 99.9%. Both HRS spectrometers were used to double the statistics and constrain the systematic uncertainties by comparing the cross sections extracted using each HRS. The proton and deuteron results are from Hall B [25], where there is the CEBAF Large Acceptance Spectrometer (CLAS) and Hall C, where there are the High Momentum Spectrometer (HMS) and the Short Orbit Spectrometer (SOS). Polarized solid NH_3 and ND_3 targets [26] using dynamical nuclear polarization were used. Polarizations up to 95% for NH_3 and up to 45% for ND_3 were achieved.

2.1 Results of the generalized GDH sum and BC sum for ^3He and the neutron

Fig. 1 shows the extended GDH integrals $I(Q^2) = \int_{\nu_{thr}}^{\infty} [\sigma_{1/2}(Q^2) - \sigma_{3/2}(Q^2)] d\nu / \nu(Q^2)$ (open circles) for ^3He (preliminary) (upper-left) and for the neutron (upper-right), which were extracted from Hall A experiment E94-010[6], from break-up threshold for ^3He (from pion threshold for the neutron) to $W = 2$ GeV. The uncertainties, when visible, represent statistics only; the systematics are shown by the grey band. The solid squares include an estimate of the unmeasured high-energy part. The corresponding uncertainty is included in the systematic uncertainty band. The preliminary ^3He results rise with decreasing Q^2 . Since the GDH sum rule at $Q^2 = 0$ predicts a large negative value, a drastic turn around should happen at Q^2 lower than 0.1 GeV^2 . A simple model using MAID [18] plus quasielastic contributions estimated from a PWIA model [42] indeed shows the expected turn around. The data at low Q^2 should be a good test ground for few-body Chiral Perturbation Theory calculations.

The neutron results indicate a smooth variation of $I(Q^2)$ to increasingly negative values as Q^2 varies from 0.9 GeV^2 towards zero. The data are more negative than the MAID model calculation[18]. Since the calculation only includes contributions to $I(Q^2)$ for $W \leq 2 \text{ GeV}$, it should be compared with the open circles. The GDH sum rule prediction, $I(0) = -232.8 \mu\text{b}$, is indicated in Fig. 1, along with extensions to $Q^2 > 0$ using two next-to-leading order χPT calculations, one using the Heavy Baryon approximation ($\text{HB}\chi\text{PT}$) [37] (dotted line) and the

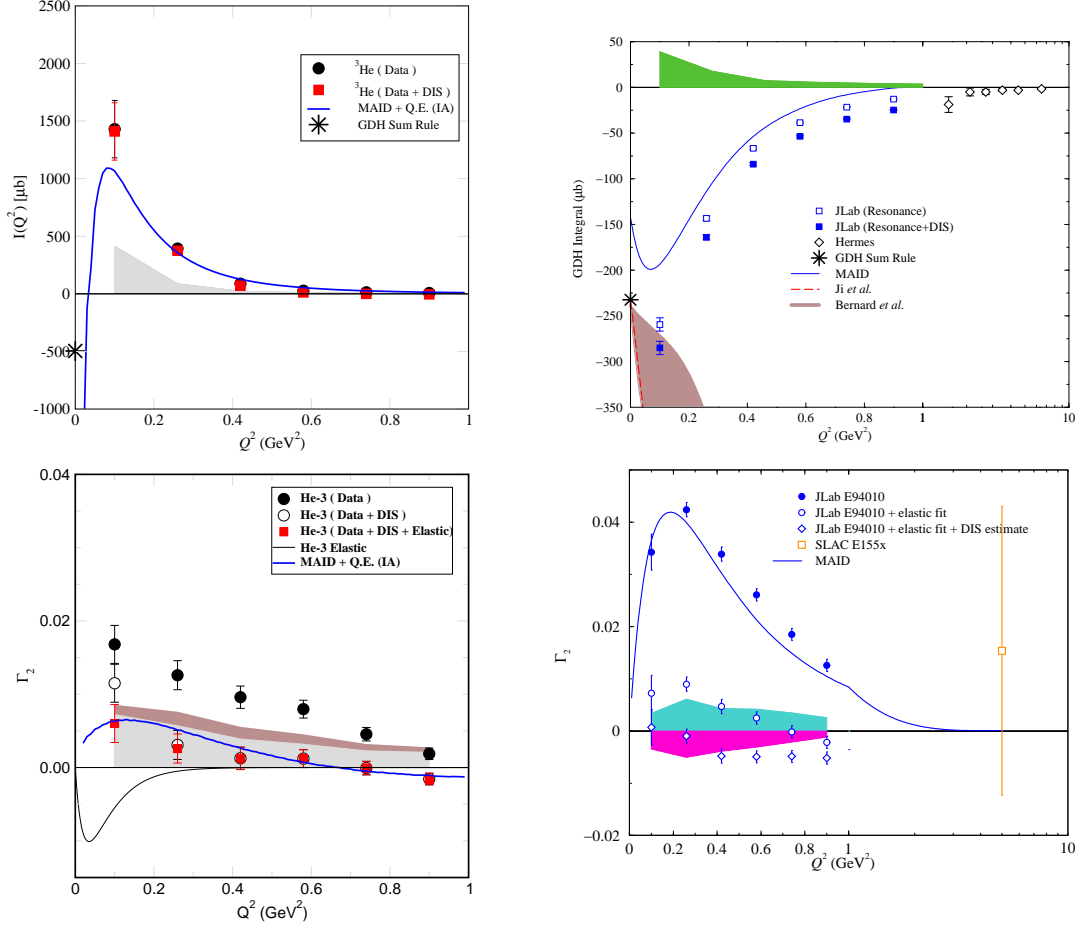


Fig. 1. Results of GDH sum $I(Q^2)$ and BC sum $T_2(Q^2)$ for ${}^3\text{He}$ [7] and the neutron [6]. The ${}^3\text{He}$ GDH results are compared with the MAID model plus quasielastic contribution. The neutron GDH results are compared with χ PT calculations of ref. [37] (dotted line) and ref. [39] (dot-dashed line). The MAID model calculation of ref. [18], is represented by a solid line. Data from HERMES [23] are also shown. The BC sum results (resonance only) are compared with MAID model calculations.

other Relativistic Baryon χ PT (RB χ PT) [39] (dot-dashed line). Shown with a grey band is RB χ PT including resonance effects [39], which have an associated large uncertainty due to the resonance parameters used.

The capability to transversely polarize the Hall A ${}^3\text{He}$ target allows precise measurements of g_2 . The integral of $\Gamma_2^{3He} = \int_0^\infty g_2^{3He}(Q^2)dx$ and Γ_2^n is plotted in the lower-left and lower-right panels of Fig. 1 in the measured region (solid circles) and open circles show the results after adding an estimated DIS contribution for ${}^3\text{He}$ (elastic contribution for the neutron). The solid squares (open diamonds) correspond to the results obtained after adding the elastic contributions for ${}^3\text{He}$, (adding an estimated DIS contribution assuming $g_2 = g_2^{WW}$ for the neutron). The MAID estimate agrees with the general trend but is slightly lower than the resonance data. The two bands correspond to the experimental systematic errors and the estimate of the systematic error for the low- x extrapolation. The total results are consistent with the BC sum rule. The SLAC E155x collaboration[54] previously reported a neutron result at high Q^2 (open square), which is consistent with zero but with a rather large error bar. On the other hand, the SLAC proton result was reported to deviate from the BC sum rule by 3 standard deviations.

2.2 First moments of g_1 and the Bjorken sum

The new results from the Hall B eg1b [51] experiment on $\bar{\Gamma}_1(Q^2)$ at low to moderate Q^2 are shown together with published results from Hall A [6] and Hall B eg1a [50] in Fig. 2 along with the data from SLAC [54] and HERMES[23]. The new results are in good agreement with the

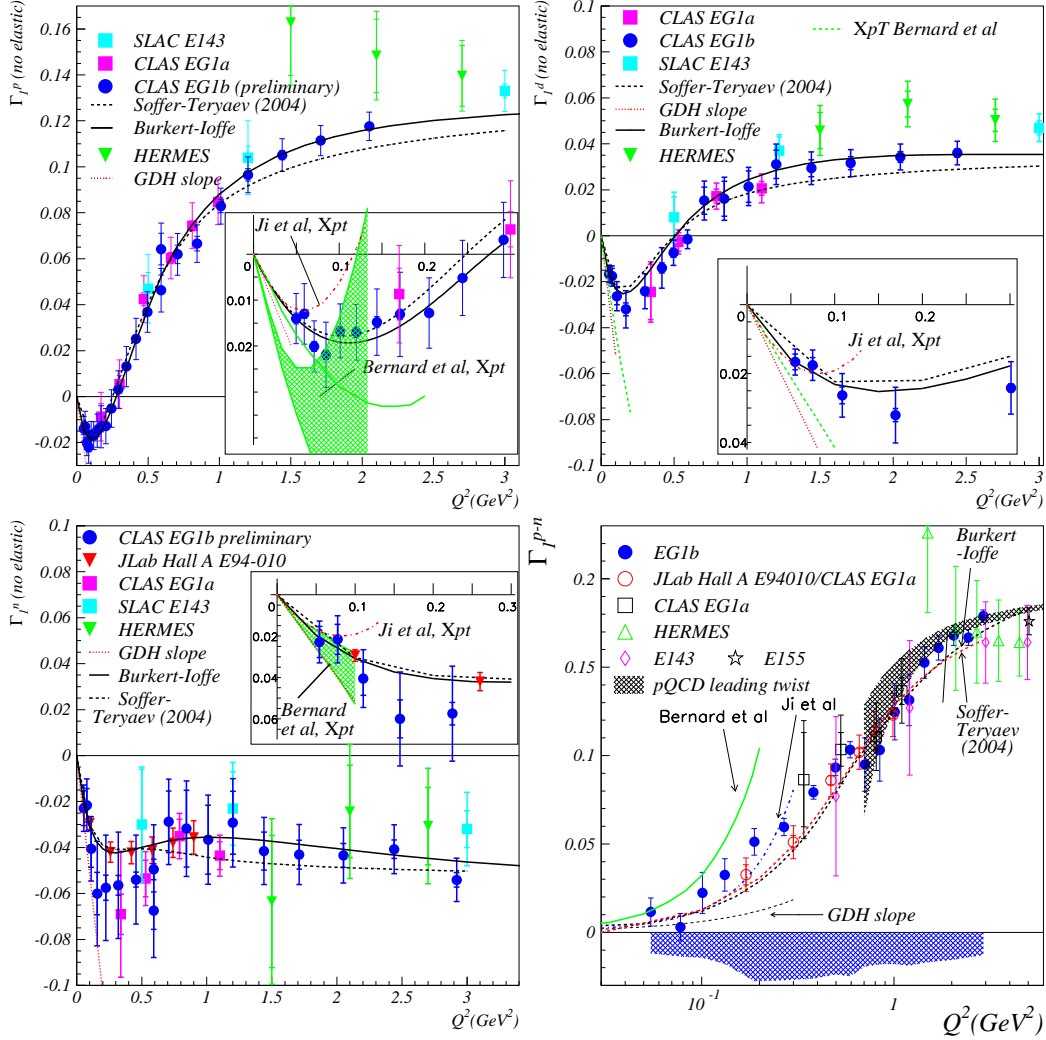


Fig. 2. Results of $\Gamma_1(Q^2)$ for p, n, d and p-n from JLab Hall A [6] and CLAS eg1a [50] and eg1b [51]. The slopes at $Q^2=0$ predicted by the GDH sum rule are given by the dotted lines. The MAID model predictions that include only resonance contributions are shown by the full lines while the dashed (dot-dashed) lines are the predictions from the Soffer-Teryaev (Burkert-Ioffe) model. The leading twist Q^2 -evolution of the moments is given by the grey band. The insets show comparisons with χ PT calculations. The full lines (bands) at low Q^2 are the next-to-leading order χ PT predictions by Ji *et al.* (Bernard *et al.*).

published data. The inner uncertainty indicates the statistical uncertainty while the outer one is the quadratic sum of the statistical and systematic uncertainties.

At $Q^2=0$, the GDH sum rule predicts the slopes of Γ_1 (dotted lines). The behavior at low Q^2 can be calculated with χ PT. We show results of calculations by Ji *et al.* [37] using HB χ PT and

by Bernard *et al.* with and without [39] the inclusion of vector mesons and Δ degrees of freedom. The calculations are in reasonable agreements with the data at the lowest Q^2 settings of 0.05 - 0.1 GeV². At moderate and large Q^2 data are compared with two model calculations [56,57]. Both models agree well with the data. The leading-twist pQCD evolution is shown by the grey band. It tracks the data down to surprisingly low Q^2 , which indicates an overall suppression of higher-twist effects.

The lower-right panel in Figure 2 shows the moment of $g_1^p - g_1^n$, the generalized Bjorken sum. This is of special interest because it contains contributions only from the flavor non-singlet (or isovector) part. The data at high Q^2 value were used to test the Bjorken sum rule as one of the fundamental tests of QCD. They were also used to extract a value of strong coupling constant, α_s . The new JLab data at low Q^2 provide interesting information in the low energy region, where the strong interaction is truly strong and non-perturbative. A new attempt [45] was made to extract an effective strong coupling, α_s^{eff} in the low Q^2 region (Figure 3). The extracted α_s^{eff} shows a clear trend of weakening Q^2 -dependence with decreasing Q^2 . With the GDH sum rule as a limit at $Q^2 = 0$, a model fit through the extracted α_s^{eff} show a loss of Q^2 -dependence as Q^2 approaches zero. This is consistent with a conformal behavior, which is important for any attempt to apply AdS/CFT [46] for the strong interaction in the low-energy region.

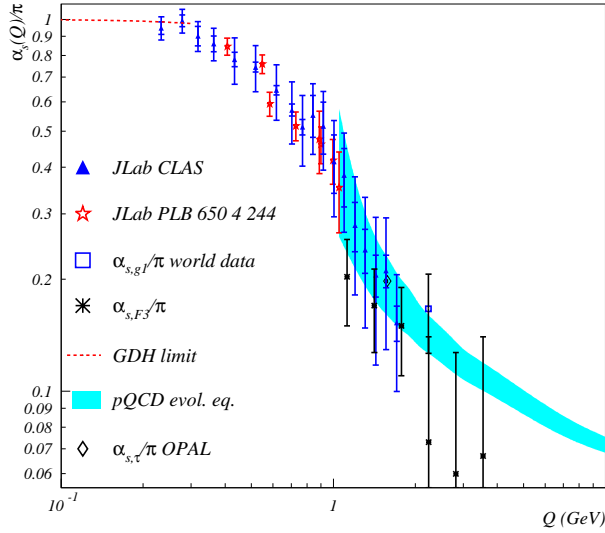


Fig. 3. Results of α_s^{eff} [45] extracted from generalized Bjorken sum, together with world data on α_s^{eff} and a model fit.

2.3 Spin Polarizabilities: γ_0 and δ_{LT}

The generalized spin polarizabilities provide benchmark tests of χ PT calculations at low Q^2 . Since the generalized polarizabilities have an extra $1/\nu^2$ weighting compared to the first moments (GDH sum or I_{LT}), these integrals have less contributions from the large- ν region and converge much faster, which minimizes the uncertainty due to the unmeasured region at large ν .

At low Q^2 , the generalized polarizabilities have been evaluated with next-to-leading order χ PT calculations [38,39]. One issue in the χ PT calculations is how to properly include the nucleon resonance contributions, especially the Δ resonance. As was pointed out in Refs. [38,39]

, while γ_0 is sensitive to resonances, δ_{LT} is insensitive to the Δ resonance. Measurements of the generalized spin polarizabilities are an important step in understanding the dynamics of QCD in the chiral perturbation region.

The first results for the neutron generalized forward spin polarizabilities $\gamma_0(Q^2)$ and $\delta_{LT}(Q^2)$ were obtained at Jefferson Lab Hall A [6].

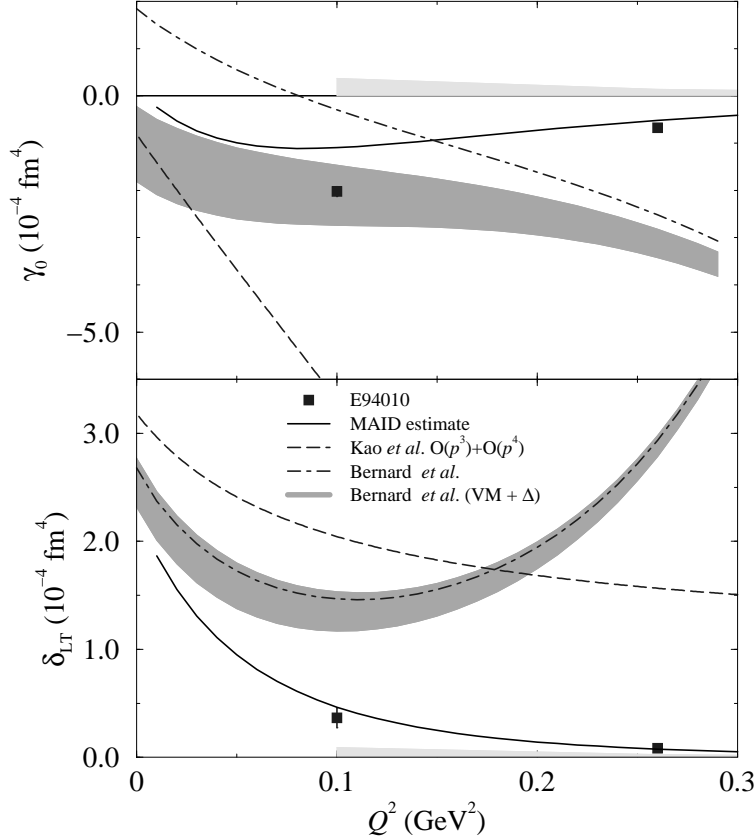


Fig. 4. Results for the neutron spin polarizabilities γ_0 (top-panel) and δ_{LT} (bottom-panel). Solid squares represent the results with statistical uncertainties. The light bands represent the systematic uncertainties. The dashed curves represent the heavy baryon χ PT calculation [38]. The dot-dashed curves and the dark bands represent the relativistic baryon χ PT calculation without and with [39] the Δ and vector meson contributions, respectively. Solid curves represent the MAID model [18].

The results for $\gamma_0(Q^2)$ are shown in the top-left panel of Fig. 4. The statistical uncertainties are smaller than the size of the symbols. The data are compared with a next-to-leading order ($O(p^4)$) HB χ PT calculation [38], a next-to-leading order RB χ PT calculation and the same calculation explicitly including both the Δ resonance and vector meson contributions [39]. Predictions from the MAID model [18] are also shown. At the lowest Q^2 point, the RB χ PT prediction including the resonance contributions is in good agreement with the experimental result. For the HB χ PT calculation without explicit resonance contributions, discrepancies are large even at $Q^2 = 0.1 \text{ GeV}^2$. This might indicate the significance of the resonance contributions or a problem with the heavy baryon approximation at this Q^2 . The higher Q^2 data point is in good agreement with the MAID prediction, but the lowest data point at $Q^2 = 0.1 \text{ GeV}^2$ is significantly lower. Since δ_{LT} is insensitive to the Δ resonance contribution, it was believed that δ_{LT} should be more suitable than γ_0 to serve as a testing ground for the chiral dynamics of QCD [38,39]. The bottom-left panel of Fig. 4 shows δ_{LT} compared to χ PT calculations and

the MAID predictions. While the MAID predictions are in good agreement with the results, it is surprising to see that the data are in significant disagreement with the χ PT calculations even at the lowest Q^2 , 0.1 GeV². This disagreement (“ δ_{LT} puzzle”) presents a significant challenge to the present Chiral Perturbation Theory.

Results of $gamma_0$ on the proton has been recently submitted for publication [51]. They show significant disagreement with both χ PT calculations [38,39]. The isospin separation was performed and discussed in Ref. [51].

New experimental data have been taken at very low Q^2 , down to 0.02 GeV² for the neutron (³He) [47] for both longitudinal and transverse target polarizations, for the proton and deuteron [48] for only the longitudinal target polarization. Preliminary results just became available for the neutron. Analysis is underway for the proton and deuteron data. These results will shed light and provide benchmark tests to the χ PT calculations at the kinematics where they are expected to work. A new proposal [49] was recently approved to measure g_2^p with a transversely polarized proton target in the low Q^2 region. It will provide an isospin separation of the spin polarizabilities to shed light on the “ δ_{LT} ” puzzle.

2.4 Precision measurements of A_1 in the high- x region and polarized valence quark distribution

JLab Hall A experiment E99-117 [3] measured A_1^n with high precision in the x region from 0.33 to 0.61 (Q^2 from 2.7 to 4.8 GeV²). Asymmetries from inclusive scattering of a highly polarized 5.7 GeV electron beam on a high pressure (> 10 atm) (both longitudinally and transversely) polarized ³He target were measured. Parallel and perpendicular asymmetries were extracted for ³He. After taking into account the beam and target polarizations and the dilution factor, they were combined to form A_1^{3He} . Using the most recent model [27], nuclear corrections were applied to extract A_1^n . The results on A_1^n are shown in the left panel of Fig. 5.

The experiment greatly improved the precision of data in the high- x region, providing the first evidence that A_1^n becomes positive at large x , showing clear SU(6) symmetry breaking. The results are in good agreement with the LSS 2001 pQCD fit to previous world data [28] (solid curve) and the statistical model [29] (long-dashed curve). The trend of the data is consistent with the RCQM [12] predictions (the shaded band). The data disagree with the predictions from the leading-order pQCD models [13] (short-dashed and dash-dotted curves). These data provide crucial input for the global fits to the world data to extract the polarized parton distribution functions and the extractions of higher-twist effects.

New results of A_1^p and A_1^d from the Hall B eg1b experiment [51] have recently become available. The data cover the Q^2 range of 1.4 to 4.5 GeV² for x from 0.2 to 0.6 with an invariant mass larger than 2 GeV. The precision of the data improved significantly over that of the existing world data.

In the leading-order approximation, the polarized quark distribution functions $\Delta u/u$ and $\Delta d/d$ were extracted from the Hall A neutron data, the CLAS eg1b proton and deuteron data and the world data. The results are shown in the right panel of Fig. 5, along with predictions from the leading-order pQCD (short-dashed curves) and pQCD fit including quark orbital angular momentum contributions [30]. The results of $\Delta d/d$ are in significant disagreement with the predictions from a leading-order pQCD model assuming hadron helicity conservation. Data agree much better with the fit including quark-orbital angular momentum contributions, suggesting that the quark orbital angular momentum may play an important role in this kinematic region.

2.5 Precision g_2 measurements and higher twist effects

A precision measurement of g_2^n from JLab Hall A E97-103 [4] covered five different Q^2 values from 0.58 to 1.36 GeV² at $x \approx 0.2$. Results for g_2^n are given in the left panel of Fig. 6. The light-shaded area in the plot gives the leading-twist contribution, obtained by fitting world

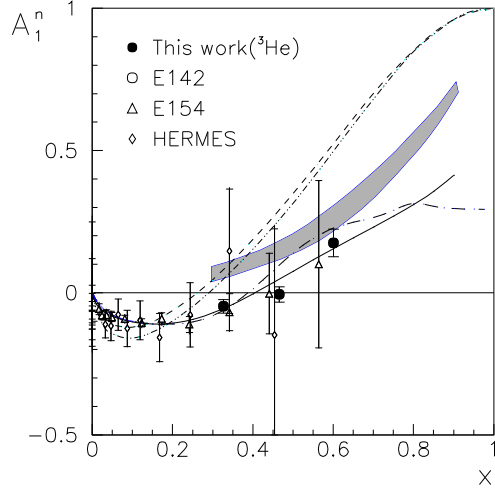


Fig. 5. A_1^n (left-panel), $\Delta u/u$ (upper side of the right-panel) and $\Delta d/d$ (lower side of the right-panel) results from JLab Hall A E99-117 [47] and CLAS eg1b [51] experiments, compared with the world data, the JLab 12 GeV projections (open points) [70] and theoretical predictions [30].

data[32] and evolving to the Q^2 values of this experiment. The systematic errors are shown as the dark-shaded area near the horizontal axis.

The precision reached is more than an order of magnitude improvement over that of the

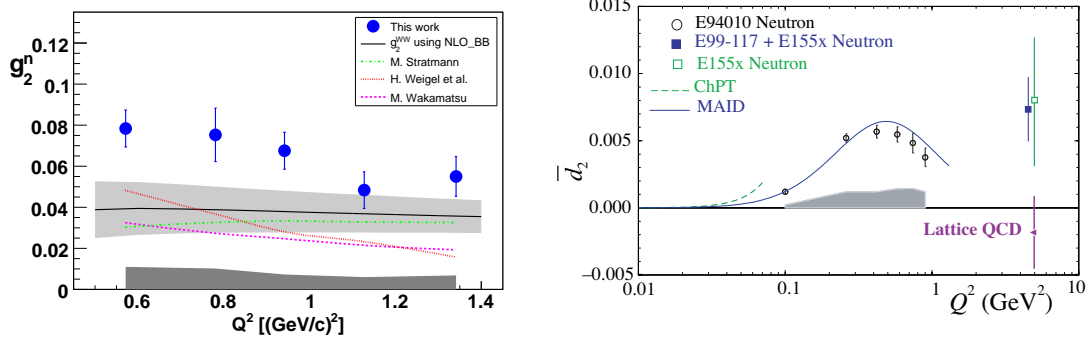


Fig. 6. Results for g_2^n (left panel) from JLab Hall A [4], in comparison with g_2^{WW} and model predictions. The right panel shows the \bar{d}_2^n results from JLab Hall A [6,3] and SLAC [54], together with the Lattice QCD calculations [36].

best world data [31]. The difference of g_2 from the leading twist part (g_2^{WW})[15] is due to higher-twist effects and is sensitive to quark-gluon correlations. The measured g_2^n values are consistently higher than g_2^{WW} . For the first time, there is a clear indication that higher-twist effects become significantly positive at Q^2 below 1 GeV^2 , while the bag model [33] and Chiral Soliton model [34,35] predictions of higher-twist effects are negative or close to zero. The g_1^n

data obtained from the same experiment agree with the leading-twist calculations within the uncertainties.

The second moment of the spin-structure function d_2 is of special interest: at high Q^2 , it is a twist-3 matrix element and can be calculated in lattice QCD. Experimentally, due to x^2 weighting, the contributions are dominated by the high- x region and the problem of low- x extrapolation is avoided. The Hall A experiment E99-117 also provided data on A_2^n at high- x . The precision of the A_2^n data is comparable to that of the best existing world data [31] at high x . Combining these results with the world data, the second moment d_2^n was extracted at an average Q^2 of 5 GeV². Compared to the previously published result [31], the uncertainty on d_2^n has been improved by about a factor of 2. The d_2 moment at high Q^2 has been calculated by Lattice QCD[36] and a number of theoretical models. While a negative or near-zero value was predicted by Lattice QCD and most models, the new result for d_2^n is positive. Also shown in Fig. 2 are the low Q^2 (0.1-1 GeV²) results of the inelastic part of d_2^n from another Hall A experiment E94-010 [6], which were compared to a Chiral Perturbation Theory calculation [37] and a model prediction[40].

A Hall C experiment [10] measured g_2 on the proton and extracted d_2^p at a Q^2 value of 1.3 GeV². A more comprehensive measurement of g_2^p and d_2^p is planned in Hall C [11] later this year. It will cover a wide Q^2 range from 2.5 to 6.5 GeV².

2.6 New results on spin-structure functions for quark-hadron duality study

JLab E01-012 [9] ran successfully in early 2003 in Hall A. Asymmetries and cross sections were measured in the resonance region, in a Q^2 range from 1 to 3.6 GeV², for inclusive scattering of polarized electrons on a longitudinally and transversely polarized ³He target. The spin-structure function g_1 and virtual photon asymmetry A_1 were extracted. The results for A_1^{3He} are presented in Fig. 7 (left panel). Also plotted are the world DIS data and a fit of the DIS data. It is interesting to note that the two sets of resonance data at the highest Q^2 agree well, indicating little or no Q^2 -dependence, which is a key feature of the DIS data. These data also show the trend of becoming positive at the high- x side, the same trend as observed for DIS data. The resonance data were integrated to study the global duality. Figure 5 (right panel) shows the results for both ³He and the neutron in comparison with the DIS fits evolved to the same Q^2 . The resonance data agree with the DIS fits at least for Q^2 higher than 1.8 GeV², indicating that the global duality holds for the neutron and ³He spin structure function, g_1 , in the high Q^2 region.

Results have also become available from the JLab Hall C experiment E01-006 [10] and Hall B experiment eg1b [51] on the proton and deuteron spin structure in the resonance region. These data, combined with the world DIS data, demonstrated that global quark-hadron duality holds in the proton and deuteron spin structure function at high Q^2 (> 1.7 GeV²), while local duality seems violated in the Δ resonance region even for Q^2 values as high as 5 GeV².

3 A planned measurement of neutron transversity at JLab

A recently approved JLab experiment [67] plans to measure the single-spin asymmetry of the $\mathbf{n}(e, e'\pi^\pm)X$ reaction on a transversely polarized ³He target. The goal of this experiment is to provide the first measurement of the neutron transversity, complementary to the HERMES and COMPASS measurements on the proton and deuteron. This experiment focuses on the valence quark region, $x = 0.19 - 0.34$, at $Q^2 = 1.77 - 2.73$ GeV². Data from this experiment, when combined with data from HERMES [65], COMPASS [61] and Belle [66], will provide powerful constraints on the transversity distributions of both u -quarks and d -quarks in the valence region.

The experiment will use a 6 GeV electron beam with the Hall A left-side high-resolution spectrometer (HRS_L) situated at 16° as the hadron arm, and the BigBite spectrometer located at 30° beam-right as the electron arm. A set of vertical coils will be added to the polarized

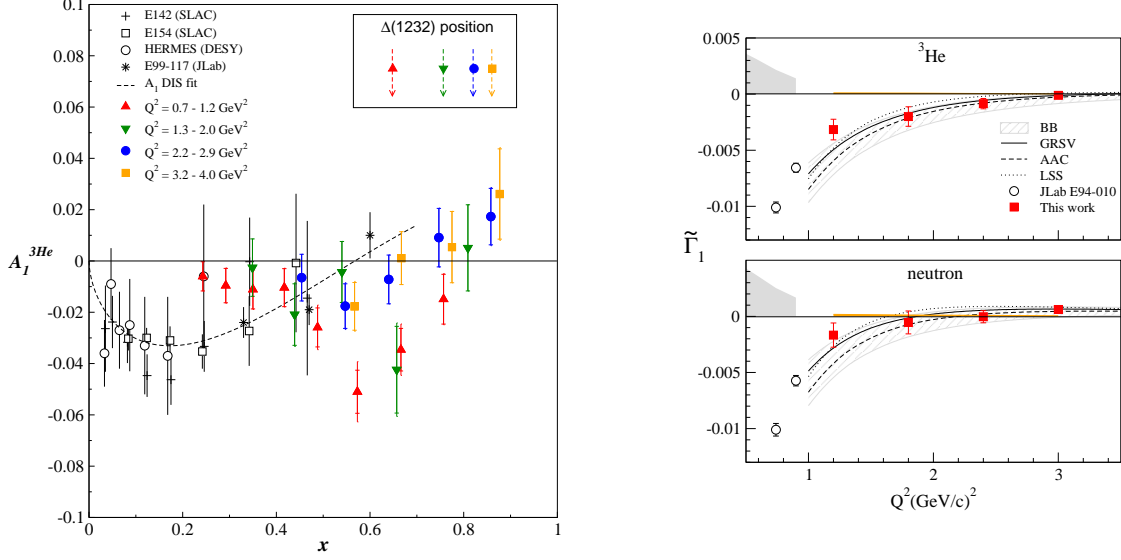


Fig. 7. A_1^{3He} (left panel) in the resonance region from JLab E01-012, compared with the world DIS data and a fit. I_1^{3He} and I_1^n (right panel) of the resonance region from JLab E01-012, together with lower Q^2 results from JLab E94-010, compared with the world DIS fits.

^3He target to provide tunable polarization directions in all three dimensions. By rotating the target polarization direction in the transverse plane, the coverage in ϕ_s^l is increased, hence facilitating the separation of the Collins and the Sivers effects. Figure 8 shows the expected statistical precision of this experiment with 29 days of beamtime for the $\mathbf{n}(e, e'\pi^\pm)X$ single-spin asymmetry. Due to the good particle identification in the HRS, K^\pm data will be collected at the same time, providing a set of precision data to study the transverse spin asymmetries for semi-inclusive K^\pm production.

4 Spin-structure program with the JLab 12 GeV energy upgrade

The JLab 12 GeV energy upgrade is the number 1 recommendation for future facilities in the US Nuclear Physics Long Range Plan published in December 2007 [68]. It has passed the US Department of Energy's Critical Decision 2 (CD2) review and is in the final stage of engineering design. It is scheduled to start physics data taking in 2014. The energy upgrade opens up a much wider DIS kinematics region to study nucleon spin structure. Planned experiments [70] in the high- x region will definitively establish the contributions of valence quarks to the nucleon structure. A precision measurement of the moment d_2 [69], part of the the color polarizabilities, will provide a benchmark test of Lattice QCD predictions. An extensive SIDIS program [71] with transversely polarized neutron and proton targets will map out precisely the Collins and Sivers moments. Together with a world-wide effort, transversity distributions functions, Sivers distribution function and Collins-fragmentation functions will be extracted. The tensor charge, a fundamental quantity of the nucleon, will be determined, which will provide a new benchmark test of Lattice QCD predictions.

A new facility, a Electron-Ion Collider (EIC), is undergoing discussion in the US hadronic-physics community, as a long-term future facility. It will provide unique capabilities for the study of QCD well beyond all existing facilities. It will extend the spin structure study over a very wide region.

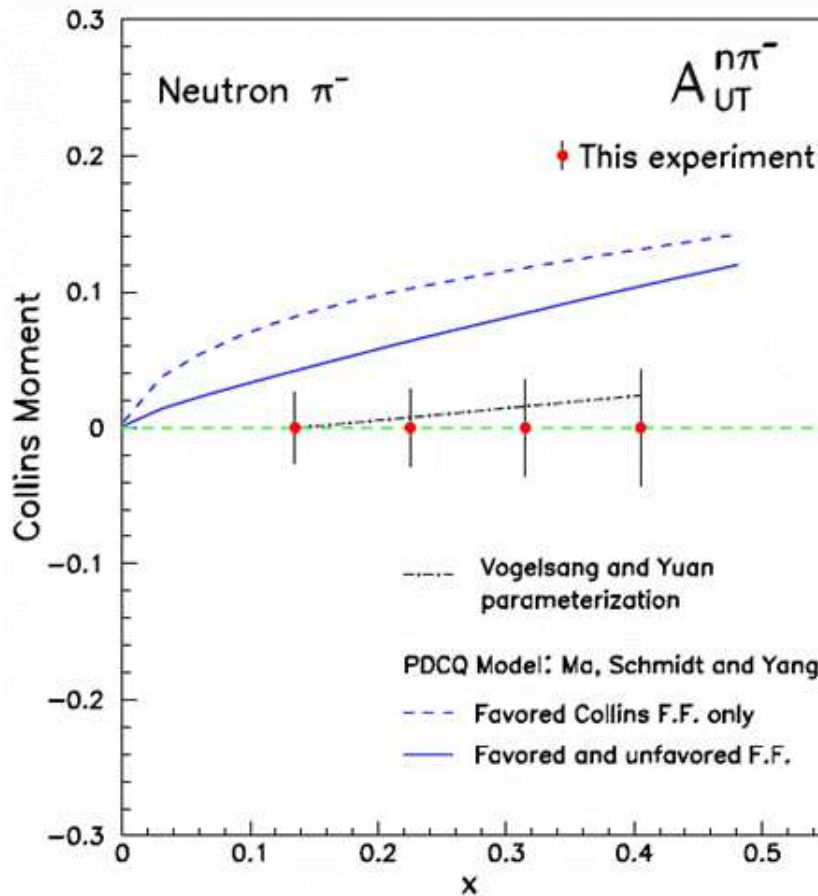


Fig. 8. Expected statistical precision of E06-010 for the Collins moment.

5 Summary

In summary, the high polarized luminosity available at JLab has provided us with high-precision data to study the nucleon spin structure in a wide kinematic range. They shed light on the valence quark structure and help to understand quark-gluon correlations and study the non-perturbative region and the transition between perturbative and non-perturbative regions of QCD. A planned precision study on transverse spin phenomena will open a new window to study the nucleon structure and help understand the strong interaction.

The work presented was supported in part by the U. S. Department of Energy (DOE) contract DE-AC05-84ER40150 Modification NO. M175, under which the Southeastern Universities Research Association operates the Thomas Jefferson National Accelerator Facility.

References

1. see, for example, B. W. Filippone and X. Ji, *Adv. Nucl. Phys.* **26**, 1 (2001)
2. J. D. Bjorken, *Phys. Rev.* **148**, 1467 (1966); *Phys. Rev. D***1**, 465 (1970)
3. X. Zheng, *et al.*, *Phys. Rev. Lett.* **92**, 012004 (2004); X. Zheng, *et al.*, *Phys. Rev. C* **70**, 065207 (2004).
4. K. Kramer, *et al.*, *Phys. Rev. Lett.***95**,142002 (2005).
5. J. P. Chen, A. Deur and Z. E. Meziani, *Mod. Phys. Lett. A* **20**, 2745 (2005).

6. M. Amarian, *et al.*, Phys. Rev. Lett. **89**, 242301 (2002); *ibid.*, **92**, 022301 (2004); *ibid.*, **93**, 152301 (2004); Z. E. Meziani *et al.*, Phys. Lett. B **613**, 148 (2005).
7. K. Slifer, *et al.*, submitted to Phys. Rev. Lett., arXiv:0803.2267 (2008).
8. A. Deur, *et al.*, Phys. Rev. Lett. **93**, 212002 (2004); A. Deur, *et al.*, submitted to Phys. Rev. Lett., arXiv:0802.3198 (2008).
9. P. Solvignon, *et al.*, submitted to Phys. Rev. Lett., arXiv:0803.3845 (2008)
10. F. R. Wesselmann, *et al.*, Phys. Rev. Lett. **98**, 132003 (2007).
11. JLab E07-003, S. Choi, Z. E. Meziani and O. Randon, spokesperosns.
12. N. Isgur, Phys. Rev. D **59**, 034013 (1999).
13. S. Brodsky, M Burkhardt and I. Schmidt, Nucl. Phys. B**441**, 197 (1995).
14. F. Close, Nucl. Phys. B **80**, 269 (1974).
15. S. Wandzura and F. Wilczek, Phys. Lett. B **72** (1977).
16. X. Ji and W. Melnitchouk, Phys. Rev. D **56**, 1 (1997).
17. S. B. Gerasimov, Sov. J. Nucl. Phys. **2**, 598 (1965); S. D. Drell and A. C. Hearn, Phys. Rev. Lett. **162**, 1520 (1966).
18. D. Drechsel, S.S. Kamalov, and L. Tiator, Phys. Rev. D **63**, 114010 (2001).
19. X. Ji and J. Osborne, J. Phys. G **27**, 127 (2001).
20. E. D. Bloom and F. J. Gilman, Phys. Rev. Lett. **25**, 1140 (1970).
21. I. Niculescu, *et al.*, Phys. Rev. Lett. **85**, 1182 (2000); **85**, 1186 (2000).
22. W. Melnitchouk, R. Ent and C. Keppel, Phys. Rept. **406**, 127 (2005).
23. A. Airapetian, *et al.*, Phys. Rev. Lett. **90**, 092002 (2003); Eur. Phys. J. C **26**, 527 (2003); Phys. Rev. D **75**, 012007 (2007).
24. Hall A collaboration: J. Alcorn *et al.*, Nucl. Inst. Meth. A **522**, 294 (2004).
25. CLAS collaboration: B. A. Mecking *et al.*, Nucl. Inst. Meth. A **503**, 513 (2003).
26. C. D. Keith *et al.*, Nucl. Inst. Meth. A **501**, 327 (2003).
27. F. Bissey, *et al.*, Phys. Rev. C **65**, 064317 (2002).
28. E. Leader, A. V. Sidorov and D. B. Stamenov, Eur. Phys. J. C **23**, 479 (2002).
29. C. Bourrely, J. Soffer and F. Buccella, Eur. Phys. J. C **23**, 487 (2002).
30. H. Avakian, S. Brodsky, A. Deur, and Y. Feng, arXiv:0705.1553 (2007).
31. K. Abe, *et al.*, E155 collaboration, Phys. Lett. B **493**, 19 (2000).
32. J. Blümlein and H. Böttcher, Nucl. Phys. B **636**, 225 (2002).
33. M. Stratmann, Z. Phys. C **60**, 763 (1993).
34. H. Weigel, Pramana **61**, 921 (2003).
35. M. Wakamatsu, Phys. Lett. B **487**, 118 (2000).
36. M. Göckeler *et al.*, Phys. Rev. D **63**, 074506 (2001).
37. X. Ji, C. Kao, and J. Osborne, Phys. Lett. B **472**, 1 (2000).
38. C. W. Kao, T. Spitzenberg and M. Vanderhaeghen, Phys. Rev. D **67**, 016001 (2003).
39. V. Bernard, T. Hemmert and Ulf-G. Meissner, Phys. Rev. D **67**, 076008 (2003).
40. D. Drechsel, S. Kamalov and L. Tiator, Phys. Rev. D **63**, 114010 (2001)
41. C. Ciofi degli Atti and S. Scopetta, Nucl. Phys. B**404**, 223 (1997)
42. C. Ciofi degli Atti, E. Pace and G. Salme, Phys. Rev. C**51**, 1108 (1995).
43. E. Thomas and N. Bianchi, Nucl. Phys. B**82** (Proc. Suppl.), 256 (2000).
44. H. Burkhardt and W. N. Cottingham, Ann. Phys. **56**, 453 (1970)
45. A. Deur, V. Burkert, J. P. Chen and W. Korsch, Phys. Lett. B **650**,4 244 (2007); submitted to Phys. Lett. B, arXiv:0803.4119 (2008).
46. S. J. Brodsky and G. F. de Teramond, Phys. Rev. Lett. **96**, 201601 (2006).
47. JLab E97-110, Spokespersons, J. P. Chen, A. Deur and F. Garibaldi.
48. JLab E03-006, Spokespersons, M. Battaglieri, A. Deur, R. De Vita and M. Ripani.
49. JLab E08-027, Spokespersones, A. Camsonne, J. P. Chen and K. Slifer.
50. R. Fatemi *et al.*, Phys. Rev. Lett. **91**, 222002 (2003); J. Yun *et al.*, Phys. Rev. C **67**, 055204 (2003).
51. K.V. Dharmawardane *et al.*, Phys. Lett. B **641** 11 (2006); Y. Prok *et al.*, submitted to Phys. Rev. Lett, arXiv:0802.2232 (2008); P. Bosted, *et al.*, Phys. Rev. C **75**, 035203, (2007).
52. D. Drechsel, B. Pasquini and M. Vanderhaeghen, Phys. Rep. **378**, 99 (2003); D. Drechsel and L. Tiator, Ann. Rev. Nucl. Part. Sci. **54**, 69 (2004).
53. X. Ji and P. Unrau, Phys. Lett. B **333**, 228 (1994).
54. K. Abe *et al.*, Phys. Rev. D **58**,112003 (1998); P. L. Anthony, *et al.*, Phys. Lett. B **493**, 19 (2000), B **553**, 18 (2003).
55. Y. Liang *et al.*, nucl-ex/0410027.
56. J. Soffer and O. V. Teryaev, Phys. Rev. D **70**, 116004 (2004).

57. V. D. Burkert and B. L. Ioffe, Phys. Lett. **B 296**, 223 (1992).
58. JLab experiment E06-014, S. Choi, X. Jiang, Z.E. Meziani and B. Sawatzky spokespersons.
59. C. Bourrely, J. Soffer and O. V. Teryaev, Phys. Lett. **B420**, 375 (1998).
60. J. Soffer, Phys. Rev. Lett. **74**, 1292 (1995).
61. The COMPASS collaboration, Phys. Rev. Lett. **94**, 202002 (2005); Nucl. Phys. **B765**, 31-70 (2007).
62. P. Mulders and R. D. Tangerman, Nucl. Phys. **B461**, 197 (1996).
63. J. Collins, Nucl. Phys. **B396**, 161 (1993).
64. D. W. Sivers, Phys. Rev. **D41**, 83 (1990).
65. A. Airapetian, *et al.*, Phys. Rev. Lett. **94**, 012002 (2005).
66. A. Ogawa, *et al.*, Proceedings of DIS2005, AIP **792**, 949 (2005).
67. JLab E06-010, J. P. Chen, H. Gao, E. Cisbani, X. Jiang, J.-C. Peng, Spokjespersons.
68. The Nuclear Science Advisory Committee Report: "The Frontiers of Nuclear Science - A Long Range Plan", (2007)
69. JLab experiment E12-06-121, T. Averett, W. Korsch, Z.E. Meziani and B. Sawatzky, spokespersons.
70. JLab experiment E12-06-110, G. Cates, J.P. Chen, Z.E. Meziani and X. Zheng, spokespersons; JLab E12-06-109, S. Kuhn, *et al.*, spokespersons.
71. A. Afanasev, *et al.*, arXiv:hep-ph/0703288 (2007).